Applied Catalysis B: Environmental 242 (2019) 327–336

Contents lists available at ScienceDirect

Applied Catalysis B: Environmental

journal homepage: www.elsevier.com/locate/apcatb

Optimization of electrocatalytic H_2O_2 production at pilot plant scale for solar-assisted water treatment

Irene Salmerón[a,b], Konstantinos V. Plakas[c], Ignasi Sirés[d], Isabel Oller[a,b,*], Manuel I. Maldonado[a,b], Anastasios J. Karabelas[c], Sixto Malato[a,b]

[a] Plataforma Solar de Almería-CIEMAT, Ctra Senés km 4, 04200, Tabernas, Almería, Spain
[b] CIESOL, Joint Centre of the University of Almería-CIEMAT, 04120, Almería, Spain
[c] Chemical Process and Energy Resources Institute, Centre for Research and Technology – Hellas (CERTH), 6th Km Charilaou-Thermi Road, Thermi, Thessaloniki, GR 57001, Greece
[d] Laboratori d'Electroquímica dels Materials i del Medi Ambient, Departament de Química Física, Facultat de Química, Universitat de Barcelona, Martí i Franquès 1-11, 08028, Barcelona, Spain

ARTICLE INFO

Keywords:
Boron-doped diamond
Gas-diffusion electrode
Hydrogen peroxide electrogeneration
Solar photoelectro-Fenton
Wastewater treatment

ABSTRACT

This manuscript summarizes the successful start-up and operation of a hybrid eco-engineered water treatment system, at pilot scale. The pilot unit, with 100 L capacity, has been devised for the efficient electrocatalytic production of H_2O_2 at an air-diffusion cathode, triggering the formation of $^{\cdot}OH$ from Fenton's reaction with added Fe^{2+} catalyst. These radicals, in combination with those formed at a powerful boron-doped diamond (BDD) anode in an undivided cell, are used to degrade a mixture of model pesticides. The capability of the plant to produce H_2O_2 on site was initially optimized using an experimental design based on central composite design (CCD) coupled with response surface methodology (RSM). This aimed to evaluate the effect of key process parameters like current density (j) and solution pH. The influence of electrolyte concentration as well as liquid and air flow rates on H_2O_2 electrogeneration and current efficiency at optimized j and pH was also assessed. The best operation conditions resulted in H_2O_2 mass production rate of 64.9 mg min^{-1}, 89.3% of current efficiency and 0.4 kWh m^{-3} of energy consumption at short electrolysis time. Performance tests at optimum conditions were carried out with 75 L of a mixture of pesticides (pyrimethanil and methomyl) as a first step towards the elimination of organic contaminants by solar photoelectro-Fenton (SPEF) process. The combined action of homogeneous ($^{\cdot}OH$) and heterogeneous (BDD($^{\cdot}OH$)) catalysis along with photocatalysis (UV photons collected at a solar CPC photoreactor) allowed the removal of more than 50% of both pesticides in 5 min, confirming the fast regeneration of Fe^{2+} catalyst through cathodic reduction and photo-Fenton reaction.

1. Introduction

The extraordinary development of chemicals manufacturing and their widespread use in all human activities is intimately associated with contamination of aquatic environment. Water quality monitoring programs underline the seriousness of the problem worldwide and highlight the potential hazards posed by mixtures of synthetic organic contaminants (SOCs) and their metabolites in surface water and groundwater [1–4]. Typically, SOCs include solvents, preservatives, pharmaceuticals and personal care products, lubricants, dyes or active substances for plant protection [5]. Among the latter, methomyl (MET) and pyrimethanil (PYR) are ubiquitous in intensive agriculture, which is worrisome since they are classified as persistent organic pollutants (POPs) [6] and are considered extremely toxic [7,8]. This issue has prompted the application of advanced oxidation processes (AOPs) for the fast and complete removal of SOCs from polluted water streams [9], based on the in situ production of hydroxyl radical ($^{\cdot}OH$) as main reactive oxygen species (ROS).

Fenton's reaction between ferrous ions (Fe^{2+}) and hydrogen peroxide (H_2O_2), so-called Fenton's reagent, is the most popular source of $^{\cdot}OH$ for practical applications [10]. As an upgraded approach, the electro-Fenton (EF) process allows overcoming two key limitations of the conventional chemical method [11–13]: (i) it ensures the continuous regeneration of Fe^{2+} through cathodic reduction of Fe^{3+}, thus requiring a much lower amount of catalyst to perform the treatment, and (ii) it avoids the handling, storage and transportation of H_2O_2 produced industrially, since this reagent can be electrosynthesized on site through Reaction (1) by using appropriate cathode materials.

* Corresponding author.
E-mail address: isabel.oller@psa.es (I. Oller).

https://doi.org/10.1016/j.apcatb.2018.09.045
Received 12 June 2018; Received in revised form 11 September 2018; Accepted 15 September 2018
Available online 29 September 2018
0926-3373/ © 2018 Elsevier B.V. All rights reserved.

$$O_{2(g)} + 2H^+ + 2e^- \rightarrow H_2O_2 \quad (1)$$

Electrocatalytic H_2O_2 generation is becoming a hot topic because the combination of electrochemistry with new catalysts enables a more eco-friendly and less energy-intensive production of this commodity [14,15]. Several prospective electrocatalysts have been developed, with noble metals and metal alloys like Pd-Au, Pt-Hg and Pt/Pd-Hg as particularly prominent options [14,16,17]. Non-precious Co-based particles are very active promoters of Reaction (1) as well, at smaller cost [18]. Unfortunately, none of these catalysts is viable for large-scale water treatment due to their high cost and toxicity, which has fostered the investigation on inexpensive carbonaceous materials [14,19,20]. Unmodified carbon-based catalysts exhibit appealing characteristics as cathodes, such as non-toxicity and high stability, conductivity and durability. H_2O_2 production with such inexpensive materials is particularly interesting for developing small- or medium-size decentralized units where the chemical is generated on demand [21]. This can be achieved using graphite felt, reticulated vitreous carbon, activated carbon fiber or carbon nanotubes as cathode, completely immersed into the solution to generate H_2O_2 from dissolved O_2 [22–24]. However, much greater H_2O_2 concentrations are attained upon implementation of an air-chamber in the electrochemical reactor, since it allows continuous air-feeding through a hydrophobized carbon-based gas-diffusion electrode (GDE) [15,18,25–28]. Worth noting, the vast majority of studies on Fenton-based electrochemical AOPs (EAOPs) reporting data on H_2O_2 production at GDE have been carried out either at laboratory scale or in small pre-pilot plants of 2.5 L [29] and 5 L [30,31]. Only one work reported the use of a bigger plant with 25 L capacity, but it was mainly focused on aniline degradation [32].

Undivided electrochemical cells are preferred to perform all these studies on water treatment because the use of a separator would increase the cell voltage and hence, the energy consumption. In addition, in such cells, the combination of carbonaceous cathodes with electrocatalytic materials that promote the anodic production of heterogeneous hydroxyl radical enhances the performance of EF process. Boron-doped diamond (BDD) thin film on Si substrate is the best anode to oxidize H_2O to physisorbed $^{\cdot}OH$ via Reaction (2) [11,13,33], owing to its large overpotential for O_2 evolution. However, Ti and Nb substrates are more suitable for plant-scale applications due to their much higher mechanical and chemical resistance.

$$BDD + H_2O \rightarrow BDD(^{\cdot}OH) + H^+ + e^- \quad (2)$$

The best performance among Fenton-based EAOPs for SOCs degradation is attained upon continuous irradiation of the treated solution with UV/Vis light. This is feasible employing a UVA lamp in photoelectro-Fenton (PEF) process [11,13], since it promotes: (i) a high regeneration rate of Fe^{2+}, with concomitant production of homogeneous $^{\cdot}OH$, from photoreduction of the main Fe(III) species at pH ~ 3.0 (Reaction (3)), (ii) the photodegradation of Fe(III)-carboxylate complexes formed as intermediates (Reaction (4)), and (iii) the direct photolysis of some pollutants and/or their oxidation by-products [11,34].

$$[Fe(OH)]^{2+} + h\nu \rightarrow Fe^{2+} + {}^{\cdot}OH \quad (3)$$

$$[Fe(OOCR)]^{2+} + h\nu \rightarrow Fe^{2+} + CO_2 + R^{\cdot} \quad (4)$$

In order to achieve the synergy between electrocatalytic and photolytic reactions at an affordable cost, UVA lamps have been lately replaced by direct sunlight irradiation, yielding the promising solar PEF (SPEF) process. Its great oxidation capability arises from: (i) the higher UV photon flux from sun if the solar collector design is adapted to the photoreactor, which upgrades the $^{\cdot}OH$ production, along with (ii) the additional illumination within the visible range ($\lambda > 400$ nm), promoting Reaction (3) (also active in the visible range) and accelerating the photolysis of refractory Fe(III)-carboxylate complexes (Reaction (4)) [34]. Very good degradation results by SPEF with GDE were obtained using a recirculation small pilot plant of 2.5-L capacity equipped with a flat-plate photoreactor [35–37], also employed to treat pesticides like mecoprop [35], diuron [38] or tebuthiuron and ametryn [39]. Replacement by a more efficient photoreactor based on compound parabolic collectors (CPC) could increase the efficiency of SPEF due to the greater photon flux supply to the solution. At present, CPC is the most popular photoreactor, as confirmed by its integration in most of the SPEF units for treating 2.2 L [40], 6 L [41], 8 L [42] and up to 10 L [43–48], which is the largest volume investigated so far.

Based on the excellent performance of SPEF at limited scale, a larger pilot plant has been developed for the treatment of SOCs by EAOPs with H_2O_2 electrogeneration. The system, with capacity to treat up to 100 L, consists of four undivided Nb-BDD/GDE filter-press cells coupled with a solar CPC, and has been installed and tested at Plataforma Solar de Almería (PSA), the largest European facility to test solar technologies. As a first step toward the treatment of real wastewater, this work is focused on the optimization of pilot plant main operation variables for the electrocatalytic H_2O_2 production, including current density (j), solution pH, liquid flow rate, air flow rate and electrolyte concentration. This was made with the aid of central composite design (CCD) coupled to response surface methodology (RSM). The plant was further validated by performing degradation trials under optimum conditions using a mixture of fungicide PYR and insecticide MET spiked into conductive water at high concentrations to simulate real agricultural wastewater. Note that these pesticides have only been studied before by AOPs like solar TiO_2 photocatalysis and solar photo-Fenton at pilot scale [6] and EF at lab scale [8].

2. Materials and methods

2.1. Chemicals

Heptahydrated ferrous sulfate (Sigma-Aldrich) used as catalyst and anhydrous sodium sulfate (Fluka) employed as background electrolyte were of analytical grade. PYR (IQV, AgroEvo, 98% purity) and MET (Aragonesas Agro, 99.5% purity) were of reagent grade and used without further purification. Mixtures of the two pesticides were prepared with deionized water (conductivity < 10 μS cm^{-1}, dissolved organic carbon (DOC) < 0.5 mg L^{-1}) and the electrolyte, and their pH was adjusted with analytical grade sulfuric acid (J.T. Baker). Organic solvents and other chemicals employed for HPLC analysis of the pesticides were of analytical grade from Sigma-Aldrich.

2.2. Pilot plant

Images of the filter-press type electrochemical cells and the CPC photoreactor, along with a schematic diagram of the pilot plant, are shown in Fig. 1. The plant consisted of four plate-and-frame electrochemical reactors (Electro MP-Cells from ElectroCell) coupled to a purpose-made solar CPC. Each cell contained an anode made of BDD thin film deposited on a niobium mesh (Nb-BDD) and a carbon-polytetrafluoroethylene (PTFE) GDE as the cathode, both with 0.01 m^2 effective area. The CPC photoreactor had a total illuminated area of 2 m^2, corresponding to an irradiated volume of 23 L. It was comprised of 10 borosilicate glass tubes (150 cm length × 4.5 cm inner diameter) mounted in an aluminum frame on a platform tilted 37° (PSA, 37 °N, 2.4 °W). The working volume was 25 L to carry out the optimization of H_2O_2 electrogeneration, and 75 L to perform the degradation experiments. The unit was equipped with two magnetic drive pumps (PAN World, 0.75 kW), one for pumping the solution from the feed tank (maximum capacity of 100 L) to the electrochemical cells, and the other for the liquid recirculation to and from the CPC. The GDE was fed with compressed air (ABAC air compressor, 1.5 kW) at a pressure and flow rate regulated with a back-pressure gauge and a flowmeter, respectively, in order to avoid the flooding of the air chamber. The experiments were made at constant j using a Delta Electronika power supply (limited to 70 V and 22 A).

Global ultraviolet solar radiation (UV_G) was measured using a radiometer (Kipp & Zonen, model CUV 3) mounted on a platform tilted 37°, the

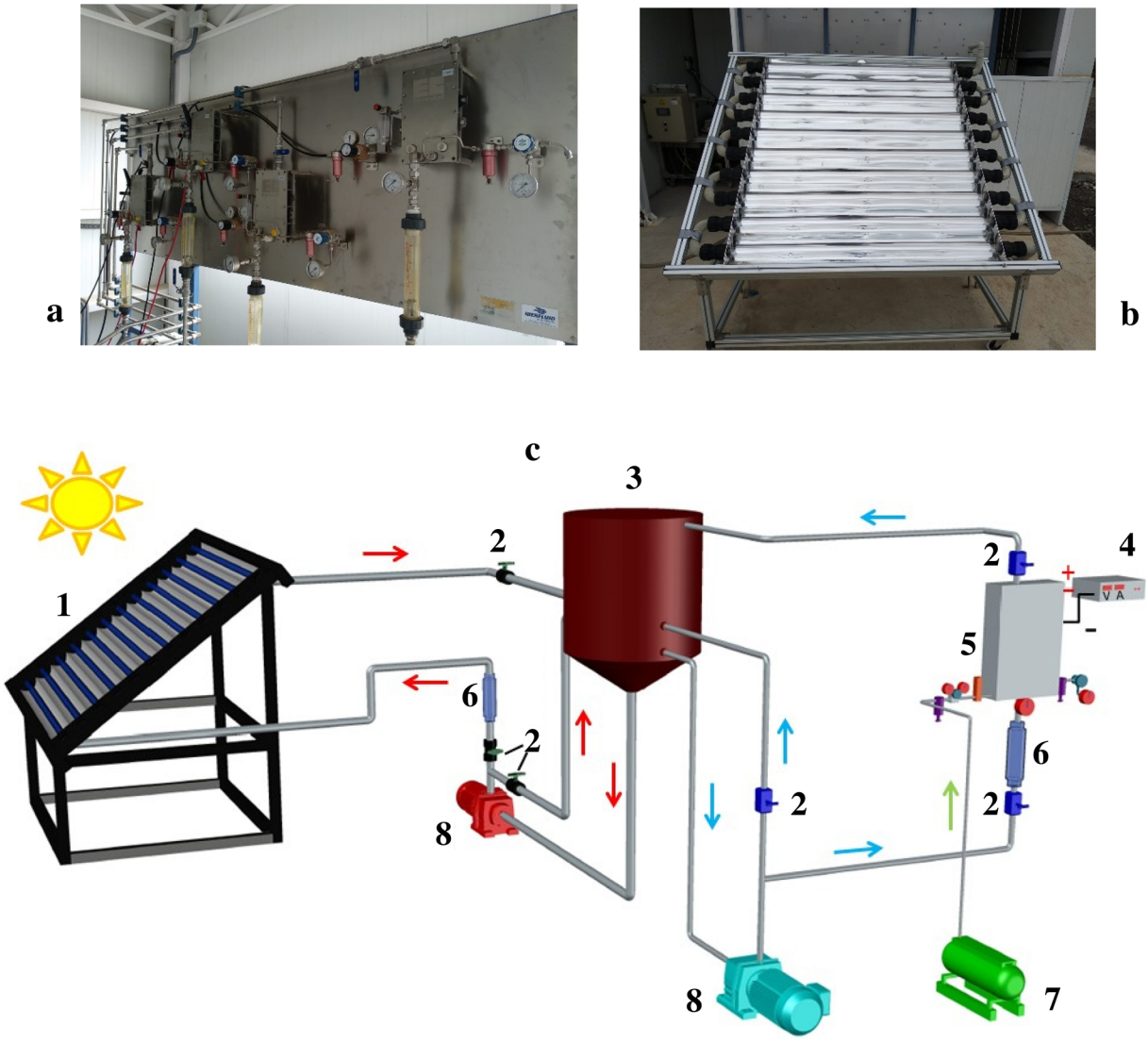

Fig. 1. Front view of (a) the four filter-press type electrochemical cells of the pilot unit, and (b) the CPC photoreactor. In (c), schematic diagram of the pilot unit equipped with one cell (examined in this work), showing: (1) CPC photoreactor, (2) valve, (3) feed tank, (4) power supply, (5) electrochemical reactor, (6) liquid flowmeter, (7) air compressor, (8) magnetic pump.

same angle as the photoreactor, which provided data in terms of incident irradiance ($W_{UV}\,m^{-2}$). This informs about the energy reaching any surface in the same position with regard to the sun. Eq. (5) allows combining the data from trials performed in different days, thus enabling comparison with results obtained in other photocatalytic experiments [49].

$$Q_{UV,n} = Q_{UV,n-1} + \Delta t_n \bullet \bar{UV}_{G,n} \bullet A_r \bullet V_T \quad (5)$$

where Q_{UV} is the accumulated UV energy per unit of volume ($kJ\,L^{-1}$), $\bar{UV}_{G,n}$ (in $W\,m^{-2}$) is the average UV radiation measured during Δt_n ($= t_n - t_{n-1}$), A_r is the irradiated surface area ($2\,m^2$) and V_T is the total volume treated in the pilot plant.

2.3. Experimental design

Experimental design by RSM was employed to optimize the in situ electrogeneration of H_2O_2. Trials were performed with one of the four identical electrochemical cells of the pilot, assuming that the resulting optimum conditions would be also valid for the other three cells. Two optimization criteria were considered: (a) maximization of the concentration of the produced H_2O_2, and (b) maximization of the current efficiency (CE, in percentage), defined as the ratio between the electricity consumed by the electrode reaction of interest and the total electricity supplied. CE can be calculated via Eq. (6), where *n* represents the stoichiometric number of electrons transferred in Reaction (1), F is the Faraday constant ($96{,}487\ C\ mol^{-1}$), $[H_2O_2]$ the concentration of H_2O_2 accumulated in bulk solution ($mg\ L^{-1}$), V_T the volume of the treated solution (L), $M(H_2O_2)$ the molecular weight of H_2O_2 ($34\,g\,mol^{-1}$), and Q the charge consumed during the electrolysis (C).

$$\%\,CE = \frac{nF\,[H_2O_2]V_T}{1000\,M(H_2O_2)Q} \times 100 \quad (6)$$

RSM was first used to assess the relationship between response (H_2O_2 concentration or % CE) and two independent variables, namely the solution pH (factor A) and *j* (factor B), as well as to optimize the relevant conditions in order to predict the best value of responses. CCD, the most widely used approach of RSM and, more specifically, a face centered composite (FCC) design, was employed to determine the effect of the two variables. Design Expert® v.7.0.0 software (Stat-Ease Inc., USA) was used. Three levels between -1 and +1 were established for the two independent variables (Table 1). Ranges were chosen based on preliminary experiments (data not shown here), background knowledge, and some constraints arising from the cathodic H_2O_2 electrogeneration and the nature of the electrode materials. For example, the production of H_2O_2 is favored at acidic pH (Reaction (2)), whereas the use of GDE and BDD

Table 1
Experimental range and levels of independent variables.

Variable	Factor	Units	Level and Range		
			Low (-1)	Central (0)	High (+1)
pH	A	–	3	5	7
j	B	mA cm^{-2}	30	65	100

anode limits the operation cell voltage to less than 25 V to prevent surface damage, which would cause the loss of electrocatalytic properties, and keep a reasonable CE [50]. This means that maximum current that can be applied is 10 A (j = 100 mA cm^{-2}).

For the CCD, a 2^3 full factorial design with 3 replicates at the center point (resulting in 19 experiments) was used to determine the optimum values of independent variables. These experiments were carried out by recirculating synthetic solutions of 50 mM Na_2SO_4 at a liquid flow rate of 4.4 L min^{-1}, and they were randomly performed to minimize the effect of systematic errors. Analysis of variance (ANOVA) of the data was performed to identify significant values (p-value < 0.05). The quality of the fit of polynomial model was expressed by the value of correlation coefficient (R^2). The main indicators demonstrating the significance and adequacy of the used model include the model F-value (Fisher variation ratio), probability value (Prob > F), and adequate precision. The optimal region of the independent variables was determined by plotting three-dimensional response surfaces of the independent and dependent variables. Additionally, numerical optimization of the independent variables was carried out using the same software.

A second set of experiments was carried out aiming to assess the effect of electrolyte concentration as well as liquid and air flow rates, under the optimum pH and j conditions. The best operation conditions were finally applied to degrade mixtures of pesticides, in the absence or presence of iron catalyst. In SPEF, the pesticide solution was irradiated when circulating through the CPC photoreactor.

2.4. Instruments and analytical methods

The concentration of H_2O_2 accumulated during the electrolysis was determined by adding Ti(IV) oxysulfate to the sample and measuring the absorbance at 410 nm, according to DIN 38,409 H15. Iron concentration was measured by using 1,10-phenanthroline, following ISO 6332. In both cases, a Unicam UV/Vis UV2 spectrophotometer was employed. Dissolved organic carbon (DOC) was measured after sample filtration through a 0.22 μm Nylon filter, on a Shimadzu TOC-VCSN analyzer. The degradation rate of the two pesticides was monitored on a UPLC/UV Agilent Technologies Series 1200, equipped with a C-18 ZORBAX XDB C-18 analytical column. The column was kept at 30 °C and the injection volume was 50 μL. A linear gradient profile with water and acetonitrile (ACN) eluted at a flow rate of 1 mL min^{-1} was established as follows: 0–4 min, isocratic at 85/15 (v/v) H_2O/ACN; 4–8 min, gradient from 85/15 to 20/80 (v/v); 8–15 min, isocratic at 85/15 (v/v). Re-equilibration time was 3 min. The UV signals for MET and PYR were monitored at the wavelength of their maximum absorption, 230 nm and 270 nm, respectively. For UPLC analyses, 9 mL of sample were filtered through a 0.22 μm PTFE syringe filter. Then, it was washed with 1 mL of UPLC grade ACN to extract any compound adsorbed on the filter. The pH of the treated solution was monitored by means of a Crison 25 pH-meter.

3. Results and discussion

3.1. Influence of independent experimental variables on the in situ H_2O_2 electrogeneration

The results obtained from the experimental design matrix including the two independent variables (pH, j) are shown in Table 2. The

Table 2
Design of experiments and results.

Run	Independent variables		Responses (t = 5 min)		Responses (t = 30 min)	
	pH	j (mA cm^{-2})	[H_2O_2] (mg L^{-1})	% CE	[H_2O_2] (mg L^{-1})	% CE
1	3	100	15.11	71.40	48.12	37.90
2	7	30	4.97	78.30	18.06	47.05
3	5	65	10.41	75.70	34.85	42.30
4	7	100	8.88	42.00	31.55	24.90
5	3	30	5.93	93.40	19.67	51.70
6	3	100	13.41	63.40	45.25	35.70
7	5	65	9.23	67.20	31.42	38.10
8	5	100	9.71	45.90	34.25	27.00
9	3	65	8.93	65.00	33.59	40.70
10	7	100	8.45	40.00	30.16	23.80
11	5	100	8.36	39.60	29.90	23.60
12	5	30	6.23	98.20	21.15	55.60
13	5	65	8.67	63.10	30.55	37.00
14	5	30	5.49	86.60	19.80	52.00
15	3	30	5.75	90.70	19.85	52.20
16	7	65	7.71	56.10	27.85	33.80
17	3	65	9.67	70.30	33.38	40.50
18	7	65	6.58	47.90	24.54	29.80
19	7	30	4.84	76.30	17.89	47.00

responses (H_2O_2 concentration and % CE) are presented at two electrolysis times, 5 and 30 min, corresponding to approximately one and five circulations of the initial feed solution volume (25 L) through the electrochemical cell, respectively. The average values of the two responses at 30 min are illustrated in Fig. 2a, whereas the changes in H_2O_2 mass production rate over the electrolysis time are depicted at constant pH = 3.0 (Fig. 2b) or j = 100 mA cm^{-2} (Fig. 2c).

As expected, a higher accumulation of H_2O_2 was found as the electrolyses were prolonged, although this occurred in concomitance with current efficiency decrease (Table 2). This is also confirmed from the profiles of the H_2O_2 production rates with time, since the highest values were attained at the beginning of the electrolyses until quasi-steady values were observed at longer times, regardless of the j (Fig. 2b) or the pH (Fig. 2c) studied. According to Eq. (6), the gradual lower efficiency with electrolysis time is related to the reduced [H_2O_2]/Q ratio as a result of nonlinear increase of the accumulated H_2O_2. This kind of behavior can be partly explained by the use of batch operation mode, since the H_2O_2 production rate at the air-diffusion cathode from Reaction (1) becomes equal to its decomposition rate by parasitic reactions that can take place in the cell. For example, the continuous recirculation of H_2O_2 accumulated in the solution may promote its electrochemical reduction at the cathode surface (Reaction (8)) and, to much lesser extent, its spontaneous disproportion in the bulk (Reaction (9)) [11].

$$H_2O_2 + 2H^+ + 2e^- \rightarrow 2H_2O \quad (8)$$

$$H_2O_2 \rightarrow ½\ O_{2(g)} + H_2O \quad (9)$$

Furthermore, considering that an undivided electrochemical reactor is employed, other additional parasitic reactions occur, as for example the oxidation of H_2O_2 to O_2 at the Nb-BDD anode surface via $HO_2^{\cdot}$ as an intermediate, according to the following reactions:

$$H_2O_2 \rightarrow HO_2^{\cdot} + H^+ + e^- \quad (10)$$

$$HO_2^{\cdot} \rightarrow O_{2(g)} + H^+ + e^- \quad (11)$$

In addition, it is worth mentioning that H_2O_2 decomposition is promoted as the solution pH becomes more alkaline, according to the following reaction:

$$H_2O_2 + OH^- \rightarrow H_2O + HO_2^- \quad (12)$$

As a consequence of these undesired reactions, the accumulated H_2O_2 concentration is always below the theoretical maximum. As explained

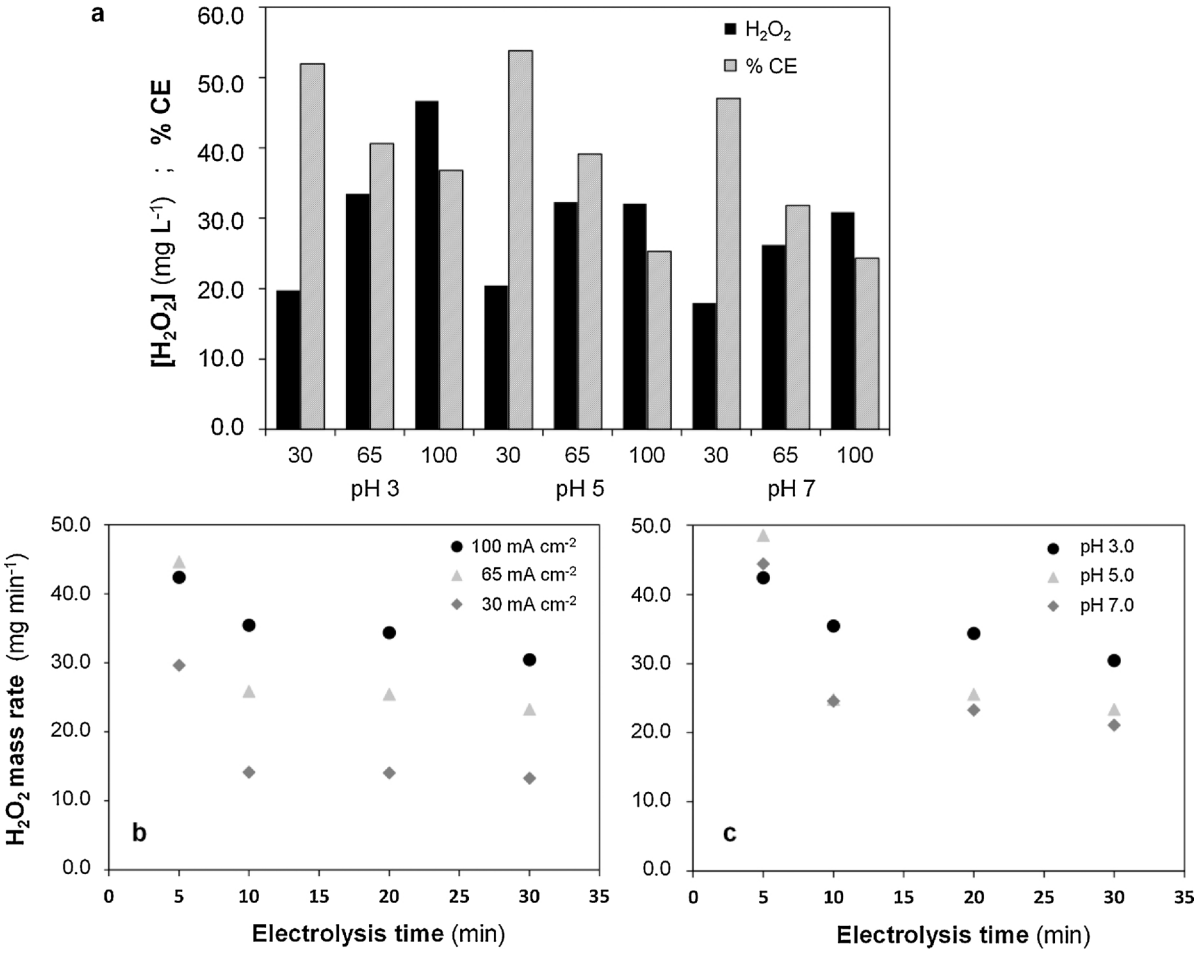

Fig. 2. (a) Accumulated H_2O_2 concentration and current efficiency (% CE) at different pH values and current densities (j). The values were obtained after 30 min of continuous recirculation of a 50 mM Na_2SO_4 solution at a liquid flow rate of 4.4 L min^{-1} and air flow rate of 5 L min^{-1}. (b) H_2O_2 production rate as function of electrolysis time, at constant pH = 3.0 and various j values. (c) H_2O_2 production rate as function of electrolysis time, at constant j = 100 mA cm^{-2} and varying pH.

in the Introduction, undivided reactors are the best choice for water treatment, but divided ones should be employed for industrial electrochemical H_2O_2 production. Note that similar trends for H_2O_2 accumulation have been reported by Brillas and co-workers, as shown during the electrolysis of Na_2SO_4 solutions in a similar batch filter-press BDD/GDE reactor at j values between 50 and 150 mA cm^{-2} [29].

In addition, Fig. 2b and c show that the maximum H_2O_2 production was achieved at 100 mA cm^{-2} and pH 3.0. This agrees with the fact that a higher electron and proton supply promotes a faster O_2 reduction from Reaction (1).

3.2. Validation of the correlation models

With the aid of Design Expert software, the models that best correlated the responses and the independent variables shown in Table 2 were:

(i) Quadratic model:

$$[H_2O_2] = 2.19 - 0.31 \cdot pH + 0.81 \cdot j - 0.05 \cdot pH \cdot j + 0.15 \cdot pH^2 - 2.42 \times 10^{-3} \cdot j^2 \quad (12)$$

- Two-factor interaction model (2FI):

$$\% \text{ CE} = 61.68 - 0.43 \cdot pH - 0.18 \cdot j - 0.0275 \cdot pH \cdot j \quad (13)$$

Both models were validated by the analysis of variances (ANOVA), and the results are summarized in Table 3. The statistical significance was assessed by means of Fisher's test. The F-values calculated for the lack of fit of the quadratic and the 2FI models were 30.44 and 60.89, respectively, suggesting that they are satisfactory. Similar conclusions can be drawn from the low probability values (p-value) at a 95% confidence level (< 0.0001) for both models. The statistical significance of the two models is also verified from Fig. 3, since the actual values of the accumulated H_2O_2 concentration and current efficiency are randomly distributed around the mean of predicted values. Moreover, good linear correlations between the predicted and observed values for H_2O_2 concentration and % CE, with corresponding R^2 values of 0.932 and 0.924, were obtained.

According to the ANOVA analysis (Table 3), the effects of the independent variables (A-pH, B-j) were obvious and the effective order was j > initial pH, whereas the interaction of the two variables (AB) was not obvious (p-value > 0.1). This can also be deduced from Fig. 2b and c, which show that the H_2O_2 production is more substantially affected by j (Fig. 2b) rather than by solution pH, with the latter showing only a slight superiority at pH 3.0 as compared to neutral pH (Fig. 2c). This is important, since the adjustment of pH when treating wastewater complicates the process and increases the water salinity and the operation cost (for acidification and subsequent neutralization).

3.3. Optimization by response surface methodology

To better assess the effect of pH and j on H_2O_2 production and current efficiency and identify their optimum values, 3D response

Table 3
ANOVA results for response surface of the Quadratic and 2FI models.

Source	Sum of squares	Degree of freedom	Mean square	F-value	p-value	
Quadratic model	1225.26	5	245.05	30.44	< 0.0001	significant
A-pH	206.75	1	206.75	25.68	0.0002	
B-*j*	880.82	1	880.82	109.41	< 0.0001	
AB	98.63	1	98.63	12.25	0.0039	
A^2	1.56	1	1.56	0.19	0.6673	
B^2	38.61	1	38.61	4.80	0.0474	
Residual	104.66	13	8.05			
Lack of fit	73.34	3	24.45	7.80	0.0056	not significant
Pure error	31.33	10	3.13			
2FI model	1723.02	3	574.34	60.89	< 0.0001	significant
A-pH	228.38	1	228.38	24.21	0.0002	
B-*j*	1466.34	1	1466.34	155.45	< 0.0001	
AB	28.31	1	28.31	3.00	0.1037	
Residual	141.49	15	9.43			
Lack of fit	102.41	5	20.48	5.24	0.0127	not significant
Pure error	39.08	10	3.91			

surfaces and contour maps were developed with the aid of Design Expert software. The response surface plot shown in Fig. 4 implies that the generation of H_2O_2 increases with j at acidic pH values. On the other hand, the current efficiency (Fig. 5) decreases as j is raised, regardless of the initial pH of the electrolyte solution. As explained above, this is attributed to the batch operation mode in an undivided cell configuration, which promotes the activation of detrimental side reactions. Four sets of optimum pH and j values were proposed by the statistical software (Table 4), yielding maximum H_2O_2 production and current efficiency. Among the four solutions proposed, solution number 1, requiring electrolyte pH = 3.0 and j = 73.66 mA cm^{-2} (~74.0), was selected as the optimum one. Under these conditions, a set of experiments was conducted aiming to validate the two correlation models (Eqs. (12) and (13)) and to investigate the effect of other operation conditions like liquid and air flow rates, as well as electrolyte concentration. The main goal was to fully optimize the electrocatalytic H_2O_2 production at plant scale, eventually yielding the most effective (highest H_2O_2 production rate), efficient (maximum CE percentage) and profitable (lowest energy consumption) process at large scale.

The results of two replicate experiments under the aforementioned optimum conditions are summarized in Table 5. The relative errors were below 5% for both, H_2O_2 generation and % CE (3.69% and 4.38%, respectively), demonstrating the excellent fitting of the experimental results (actual values) with those predicted by the two models.

3.3.1. Effect of liquid flow rate

The feed flow rate is closely related to the hydraulic residence time (HRT) of the treated solution within the electrochemical cell. This is of great significance under continuous operation mode, where the feed solution is continuously treated and discharged. For batch operation, as is the case of the experiments carried out in this work, the recirculation flow rate does not necessarily match the HRT, but it rather affects the mixing and may create turbulent flow within the electrochemical cell. This, in turn, may intensify the mass transport induced by the higher local concentration of molecular oxygen dissolved in the aqueous phase. Indeed, when the flow rate was doubled (from 2.8 to 5.6 L min^{-1}), H_2O_2 production was gradually greater at each given time (Fig. 6b), finally increasing by 28.8% at 30 min (Fig. 6a, [H_2O_2] in mg min^{-1}). Current efficiency also increased in the same proportion, as a result of the higher H_2O_2 generation at similar charge consumption (note that energy consumption varied between 1.97 and 2.00 kWh m^{-3} for all pilot runs) (Fig. 6a).

3.3.2. Effect of air flow rate

Large feeding of air or pure O_2 to the air chamber is often needed to counterbalance the existing pressure on the wet face of the GDE, thereby avoiding flooding that would stop the H_2O_2 production. If correctly adjusted, an increase in air flow rate may upgrade the H_2O_2 accumulation. As found for the pilot plant studied in this work, a rise in

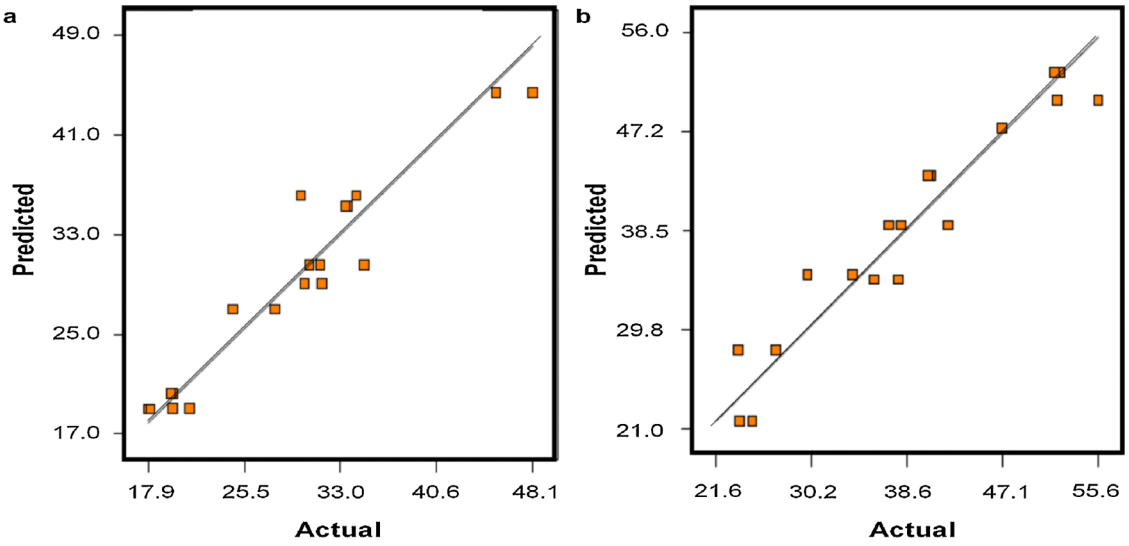

Fig. 3. Comparison of the actual results obtained experimentally regarding (a) H_2O_2 production and (b) current efficiency (in %), with those predicted via central composite design Eqs. (12) and (13), respectively.

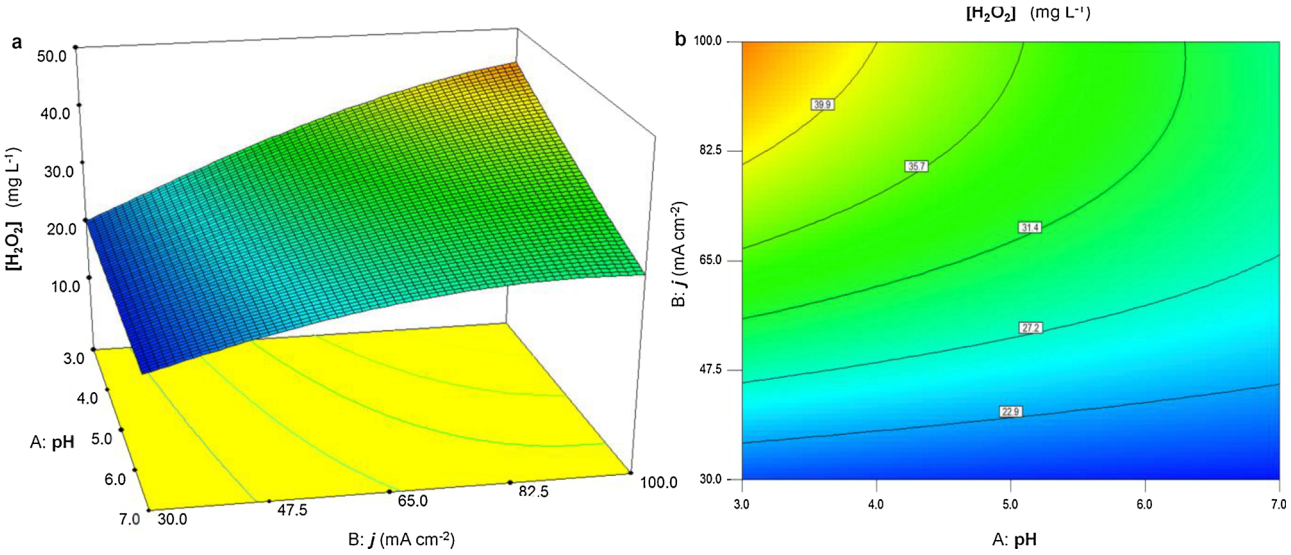

Fig. 4. (a) 3D surface plot and (b) contour plot for the H_2O_2 production as function of the initial pH (A) and current density (B). Experimental data correspond to 30-min electrolyses under continuous recirculation of a 50 mM Na_2SO_4 solution at liquid flow rate of 4.4 L min^{-1} and air flow rate of 5 L min^{-1}.

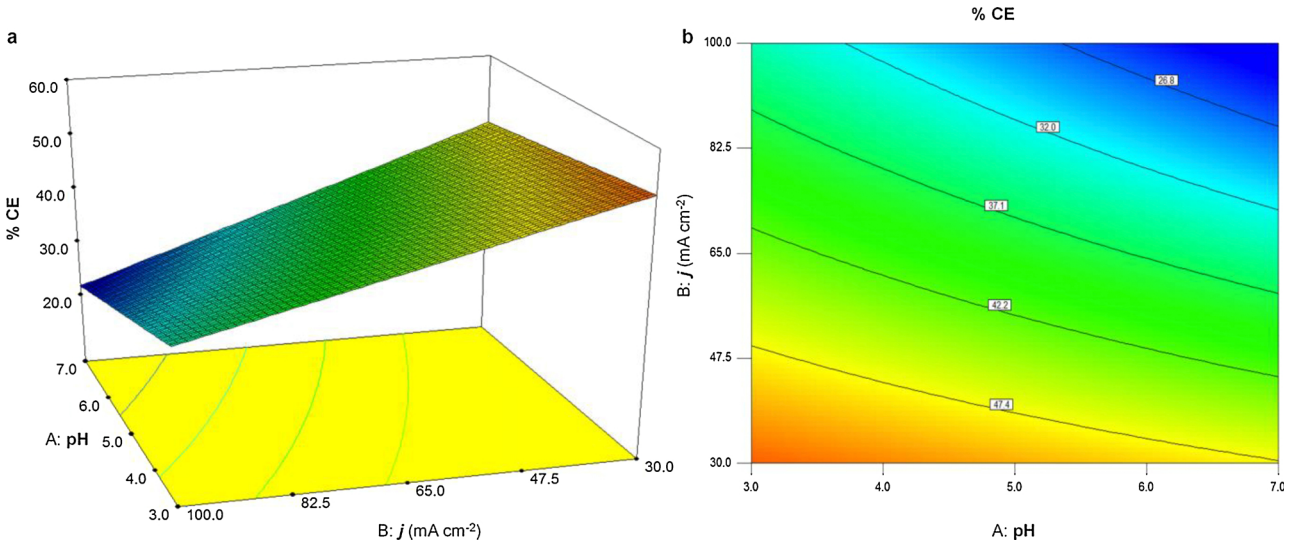

Fig. 5. (a) 3D surface plot and (b) contour plot for current efficiency (in %), as in Fig. 4.

Table 4
Optimum operation conditions proposed by Design Expert 7.0.0 software to attain maximum H_2O_2 concentration and current efficiency at 30 min of electrolysis.

Test number	pH	j (mA cm^{-2})	[H_2O_2] (mg L^{-1})	% CE	Desirability	
1	3.00	73.66	38.0961	41.0744	0.604	Selected
2	3.00	74.16	38.2467	40.9437	0.604	
3	3.00	72.82	37.8392	41.2949	0.604	
4	3.00	70.00	36.9532	42.0343	0.603	

Table 5
Models validation under optimum conditions, with experimental data obtained after 30 min of electrolysis under continuous recirculation of 50 mM Na_2SO_4 solution at pH 3.0, 74 mA cm^{-2}, liquid flow rate of 3.3 L min^{-1} and air flow rate of 5 L min^{-1}. Two independent runs were performed.

	Run		Average actual values	Predicted values	Relative error (%)
	a	b			
H_2O_2 (mg L^{-1})	35.51	38.07	36.79	38.20	3.69
% CE	37.80	40.60	39.20	40.99	4.38

the air flow rate from 2.5 and 5 L min^{-1} to 10 L min^{-1}, resulted in an enhanced H_2O_2 production by 23.1% and 15.6% at 30 min, respectively (Fig. 7a and b). Moreover, the kinetics of H_2O_2 production was faster at the maximum air flow rate of 10 L min^{-1} (Fig. 7b), with no negative effect on the corresponding energy consumption, which was similar at all air flow rates examined. This is interesting, since one might presume that an excessive air feeding could generate too many bubbles within the electrochemical reactor, thereby increasing the ohmic drop and also affecting the stability of the liquid flow rate, which did not occur.

Based on these results, as well as on the better performance of the plant at high electrolyte flow rates, it can be concluded that the combined increase of air and liquid flow rates may effectively enhance the fraction of oxygen consumed for H_2O_2 production (Reaction (1)) over the total amount of air fed. Indeed, under the optimum operation conditions, namely 50 mM Na_2SO_4 solution at pH 3.0 treated at 74 mA cm^{-2}, with liquid flow rate of 5.6 L min^{-1} and air flow rate of 10 L min^{-1}, the highest H_2O_2 mass production rate and current efficiency were

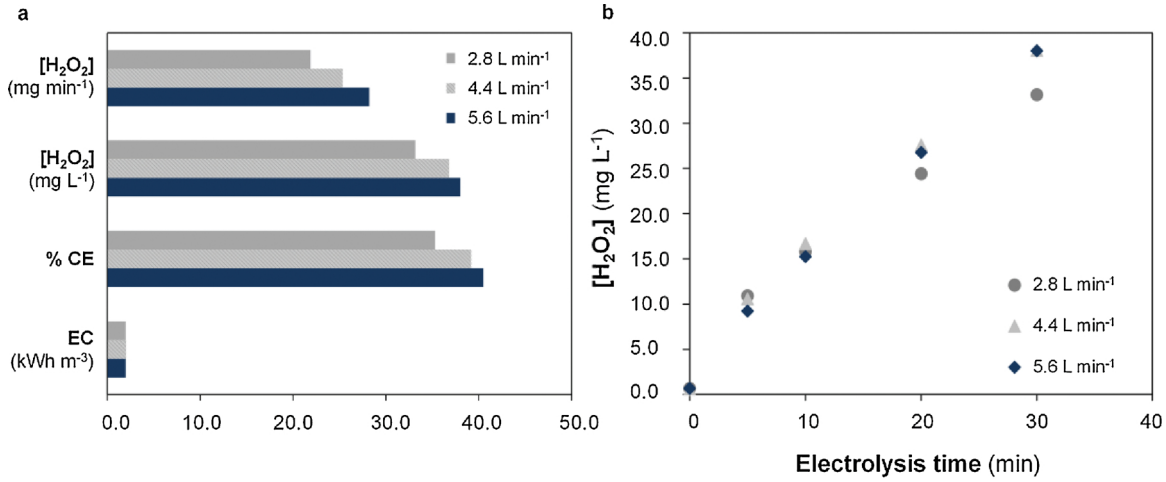

Fig. 6. (a) Effect of liquid flow rate on various process efficiency parameters, corresponding to 30-min electrolyses; (b) accumulated H_2O_2 as a function of electrolysis time, at three different liquid flow rates. Fixed parameters: 50 mM Na_2SO_4 at pH 3.0, j = 74 mA cm^{-2}, air flow rate of 5 L min^{-1}.

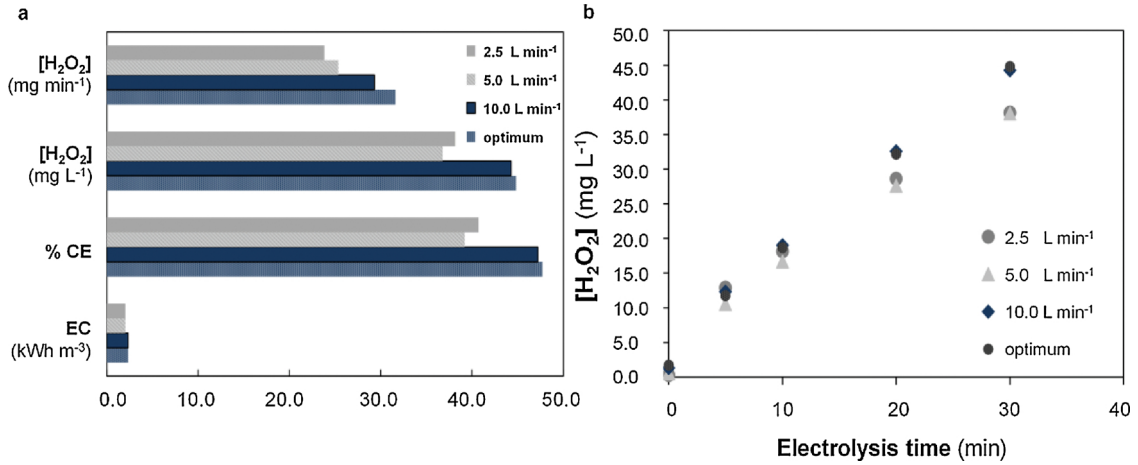

Fig. 7. (a) Effect of air flow rate on various process efficiency parameters, corresponding to 30-min electrolyses; (b) accumulated H_2O_2 as function of electrolysis time, at different air flow rates. Fixed parameters: 50 mM Na_2SO_4 at pH 3.0, j = 74 mA cm^{-2}, liquid flow rate of 4.4 L min^{-1}. The optimum trial corresponds to the same conditions but using a liquid flow rate of 5.6 L min^{-1} and air flow rate of 10 L min^{-1}.

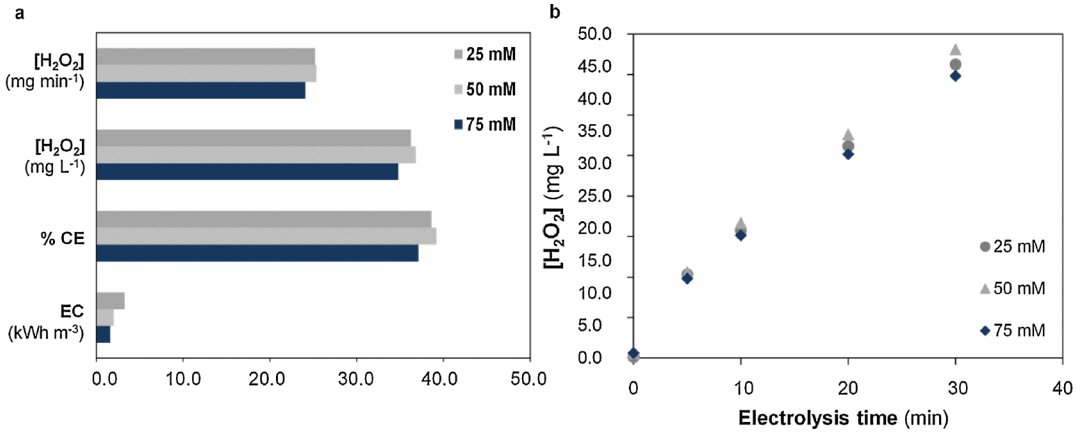

Fig. 8. (a) Effect of Na_2SO_4 molar concentration on various process efficiency parameters, corresponding to 30-min electrolyses; (b) accumulated H_2O_2 as a function of electrolysis time, at three different electrolyte concentrations. Fixed parameters: electrolyte solution at pH 3.0, j = 74 mA cm^{-2}, liquid flow rate of 4.4 L min^{-1} and air flow rate of 5 L min^{-1}.

obtained. In the first 5 min of electrolysis, these conditions led to H_2O_2 production with a mass rate of 64.9 mg min^{-1}, 89.3% current efficiency and energy consumption of 0.4 kWh m^{-3}. These values are among the best achieved with similar system configurations. For example, Flox et al. [29] reported a production rate of ca. 23 mg min^{-1} at 30 min in 50 mM Na_2SO_4 at pH 3.0, 100 mA cm^{-2} and liquid flow rate of 3 L min^{-1}, whereas Fig. 7a shows a higher H_2O_2 electrogeneration rate of 32 mg min^{-1} at that time.

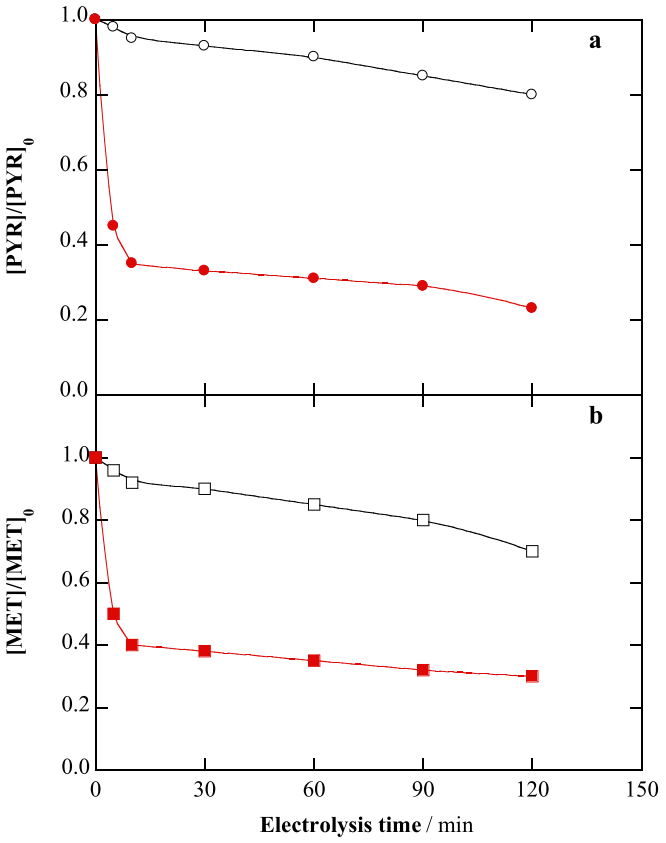

Fig. 9. Normalized concentration decays of pesticides (a) pyrimethanil (PYR) and (b) methomyl (MET) versus electrolysis time during the (○,□) electro-oxidation (EO) and (●,■) solar photoelectro-Fenton (SPEF) treatment of 75 L of mixtures of both pesticides (71 mg L^{-1} DOC) in deionized water with 50 mM Na_2SO_4 at pH 3.0 using the pilot plant at j = 74 mA cm^{-2}, liquid flow rate of 5.6 L min^{-1} and air flow rate of 10 L min^{-1}. SPEF treatment was performed in the presence of 0.5 mM Fe^{2+} as catalyst.

3.3.3. Effect of electrolyte concentration

Considering the rather small electrode gap (6 mm) between the anode and cathode in the electrochemical cell, it was assumed that the solution conductivity would not significantly affect the production of H_2O_2. Therefore, a set of experiments was made to determine the possible influence of electrolyte concentration. It was observed that, within the range of 25–75 mM of Na_2SO_4, which is equal to a solution conductivity range of 4.6–12.3 mS cm^{-1}, the accumulation of H_2O_2 was quite analogous, being only slightly higher in the case of 50 mM (Fig. 8). However, a rather substantial effect is observed regarding the energy consumption, since a higher conductivity led to a gradually lower consumption; i.e. 3.24, 2.00 and 1.61 kW h m^{-3} at 25, 50 and 75 mM Na_2SO_4, respectively. This was expected, since the increase of electrolyte concentration causes a reduction of the ohmic resistance in the bulk solution, and accelerates the electron transfer, thus decreasing the overall charge consumption. From these findings, it can be concluded that the system would be more efficient at higher water conductivity. Therefore, future industrial application of this technology should focus on high conductivity wastewater or be coupled with membrane technologies for treating membrane concentrates.

3.4. Treatment of a mixture of pesticides

After the optimum operation conditions were determined for attaining the best balance between H_2O_2 production and current efficiency, the plant performance was validated by carrying out several tests to assess its capability to degrade a mixture of two model SOCs, namely PYR and MET, which were treated by sun-assisted AOPs like solar photo-Fenton [6,51]. All the assays were made with 75 L of mixtures of both pesticides in water with 50 mM Na_2SO_4 under optimized conditions: pH 3.0, 74 mA cm^{-2} and air flow rate of 10 L min^{-1}.

First, a mixture containing 50 mg L^{-1} PYR and 90 mg L^{-1} MET (i.e., 71 mg L^{-1} DOC) was treated by EO with electrogenerated H_2O_2. The influence of liquid flow rate (2.8, 4.4 and 5.6 L min^{-1}) was investigated, aiming to promote a larger oxidation of both organic contaminants either by increasing the HRT (at a lower flow rate) or by enhancing the mass transport of pollutants to the anode surface (at a higher flow rate). However, no significant effect of this parameter was found, which suggests that the amount of BDD(˙OH) produced via Reaction (2) at 74 mA cm^{-2} was high enough to react with both pesticides regardless of the hydrodynamic conditions (within the studied range). Fig. 9a and b depict the normalized decays of PYR and MET concentrations at a liquid flow rate of 5.6 L min^{-1}, respectively. As can be seen, the degradation by EO-H_2O_2 was very slow, only attaining 20% and 30% of PYR and MET removal after 120 min. The larger degradation of MET could be explained by the greater electrocatalytic behavior of BDD with this pesticide as a result of a more favorable adsorption on its surface, thus reacting more quickly with physisorbed BDD(˙OH). At the end of the electrolysis, almost no mineralization was achieved in EO process, in agreement with the refractory nature of typical reaction by-products like carboxylic acids [10–13]. In all these trials, the energy consumption was around 10 kW h m^{-3}.

The same pesticides mixture was treated by EF, using the optimized parameters with liquid flow rate of 5.6 L min^{-1}, in the presence of different amounts of Fe^{2+} as catalyst (not shown). After 120 min, a higher degradation percentage was reached for both pesticides, with up to 35% and 40% for PYR and MET, respectively. This demonstrates that the H_2O_2 produced under optimized conditions reacted with added Fe^{2+} according to Fenton's reaction, yielding homogeneous ˙OH that enhanced the degradation because this radical acted concomitantly with BDD(˙OH). The former was confined into the reactor, whereas the latter radical was transported throughout the whole volume. In contrast, DOC abatement only attained 8% as maximum, which agrees with the high stability of Fe(III)-carboxylate complexes formed as intermediates [11]. Worth mentioning, a much larger mineralization was achieved working with a pesticide mixture that accounted for 20 mg L^{-1} DOC, using 1.0 mM Fe^{2+}. In this case, 32% DOC removal was attained at 120 min. It is also important to note that the Fe^{2+} concentration remained almost constant during all these EF trials, which confirms the capability of the cathode to regenerate it from Fe (III) reduction.

Finally, the mixtures with 71 mg L^{-1} DOC were comparatively treated by SPEF using the best Fe^{2+} concentration (i.e., 0.5 mM). In these experiments, required accumulated UV energy, Q_{UV}, was 7.1 kJ L^{-1}. As it can be observed in Fig. 9, 55% and 50% removal of PYR and MET was reached in only 5 min, which confirms the fast Fe^{2+} photoregeneration with additional ˙OH production from Reaction (3). At longer time, the degradation was much slower, but ended in 77% and 70% removal, respectively, at 120 min. This is a much better performance as compared to EO and EF, which was further confirmed by DOC abatements higher than 15%, in agreement with the powerful action of UV/Vis photons on Fe(III)-carboxylate complexes according to Reaction (4).

4. Conclusions

The successful performance of the largest SPEF pilot plant existing to date has been demonstrated in this work. The core of the plant, the filter-press electrochemical reactor, is comprised of a Nb-BDD anode and a GDE as cathode. Optimization of main operation parameters has been carried out according to a thorough experimental design, in order to maximize the electrocatalytic H_2O_2 production with a high current efficiency. Optimum values obtained for the key parameters were: pH 3.0,

74 mA cm^{-2}, liquid flow rate of 5.6 L min^{-1} and air flow rate of 10 L min^{-1}. Their application yielded a mass rate of up to 64.9 mg H_2O_2 min^{-1}, current efficiency of 89.3% and energy consumption of 0.4 kWh m^{-3} during the first minutes. The SPEF treatment of 75 L of pesticides mixtures allowed the removal of more than 50% of each pesticide in only 5 min, whereupon further degradation as well as mineralization of by-products and their Fe(III) complexes became much slower but always superior to EO and EF treatments. Further optimization of the SPEF process for treating different kind of wastewater in the integrated pilot system is in progress.

Acknowledgments

The authors wish to thank the EU funded SFERA-II project (7th Framework Programme, Grant Agreement n. 312,643), a Transnational Access program which aims at boosting scientific collaboration among the leading European institutions in solar concentration systems. Financial support from project CTQ2016-78616-R (AEI/FEDER, EU) is also acknowledged.

References

[1] R. Loos, B.M. Gawlik, G. Locoro, E. Rimaviciute, S. Contini, G. Bidoglio, Environ. Pollut. 157 (2009) 561–568.
[2] The NORMAN Network, (2012) (Accessed 15 May 2018), http://www.norman-network.net/?q=Home.
[3] J.-Q. Jiang, Z. Zhou, V.K. Sharma, Microchem. J. 110 (2013) 292–300.
[4] B. Petrie, R. Barden, B. Kasprzyk-Hordern, Water Res. 72 (2015) 3–27.
[5] C. Postigo, D. Barceló, Sci. Total Environ. 503–504 (2015) 32–47.
[6] I. Oller, S. Malato, J.A. Sánchez-Pérez, M.I. Maldonado, R. Gassó, Catal. Today 129 (2007) 69–78.
[7] D.J.E. Costa, J.C.S. Santos, F.A.C. Sanches-Brandão, W.F. Ribeiro, G.R. Salazar-Banda, M.C.U. Araujo, J. Electroanal. Chem. 789 (2017) 100–107.
[8] M. Popescu, C. Sandu, E. Rosales, M. Pazos, G. Lazar, M.A. Sanromán, J. Electroanal. Chem. 808 (2018) 455–463.
[9] C. Comninellis, A. Kapałka, S. Malato, S.A. Parsons, I. Poulios, D. Mantzavinos, J. Chem. Technol. Biotechnol. 83 (2008) 769–776.
[10] M.A. Oturan, J.-J. Aaron, Crit. Rev. Environ. Sci. Technol. 44 (2014) 2577–2641.
[11] E. Brillas, I. Sirés, M.A. Oturan, Chem. Rev. 109 (2009) 6570–6631.
[12] L. Feng, E.D. van Hullebusch, M.A. Rodrigo, G. Esposito, M.A. Oturan, Chem. Eng. J. 228 (2013) 944–964.
[13] C.A. Martínez-Huitle, M.A. Rodrigo, I. Sirés, O. Scialdone, Chem. Rev. 115 (2015) 13362–13407.
[14] S. Chen, Z. Chen, S. Siahrostami, T.R. Kim, D. Nordlund, D. Sokaras, S. Nowak, J.W.F. To, D. Higgins, R. Sinclair, J.K. Nørskov, T.F. Jaramillo, Z. Bao, ACS Sustain. Chem. Eng. 6 (2018) 311–317.
[15] T. Pérez, G. Coria, I. Sirés, J.L. Nava, A.R. Uribe, J. Electroanal. Chem. 812 (2018) 54–58.
[16] S. Siahrostami, A. Verdaguer-Casadevall, M. Karamad, D. Deiana, P. Malacrida, B. Wickman, M. Escudero-Escribano, E.A. Paoli, R. Frydendal, T.W. Hansen, Ib Chorkendorff, I.E.L. Stephens, J. Rossmeisl, Nature Mater. 12 (2013) 1137–1143.
[17] E. Pizzutilo, O. Kasian, C.H. Choi, S. Cherevko, G.J. Hutchings, K.J.J. Mayrhofer, S.J. Freakley, Chem. Phys. Lett. 683 (2017) 436–442.
[18] C. Ridruejo, F. Alcaide, G. Álvarez, E. Brillas, I. Sirés, J. Electroanal. Chem. 808 (2018) 364–371.
[19] G.-L. Chai, Z. Hou, T. Ikeda, K. Terakura, J. Phys. Chem. C 121 (2017) 14524–14533.
[20] V. Čolić, S. Yang, Z. Révay, I.E.L. Stephens, Ib Chorkendorff, Electrochim. Acta 272 (2018) 192–202.
[21] S. Yang, A. Verdaguer-Casadevall, L. Arnarson, L. Silvioli, V. Čolić, R. Frydendal, J. Rossmeisl, Ib Chorkendorff, I.E.L. Stephens, ACS Catal. 8 (2018) 4064–4081.
[22] A. Dirany, I. Sirés, N. Oturan, A. Özcan, M.A. Oturan, Environ. Sci. Technol. 46 (2012) 4074–4082.
[23] M. Panizza, A. Dirany, I. Sirés, M. Haidar, N. Oturan, M.A. Oturan, J. Appl. Electrochem. 44 (2014) 1327–1335.
[24] G. Coria, T. Pérez, I. Sirés, J.L. Nava, J. Electroanal. Chem. 757 (2015) 225–229.
[25] K.V. Plakas, S.D. Sklari, D.A. Yiankakis, G.Th. Sideropoulos, V.T. Zaspalis, A.J. Karabelas, Water Res. 91 (2016) 183–194.
[26] A. Galia, S. Lanzalaco, M.A. Sabatino, C. Dispenza, O. Scialdone, I. Sirés, Electrochem. Commun. 62 (2016) 64–68.
[27] Z.G. Aguilar, E. Brillas, M. Salazar, J.L. Nava, I. Sirés, Appl. Catal. B: Environ. 206 (2017) 44–52.
[28] S. Lanzalaco, I. Sirés, M.A. Sabatino, C. Dispenza, O. Scialdone, A. Galia, Electrochim. Acta 246 (2017) 812–822.
[29] C. Flox, J.A. Garrido, R.M. Rodríguez, P.-L. Cabot, F. Centellas, C. Arias, E. Brillas, Catal. Today 129 (2007) 29–36.
[30] G.R. Agladze, G.S. Tsurtsumia, B.-I. Jung, J.-S. Kim, G. Gorelishvili, J. Appl. Electrochem. 37 (2007) 375–383.
[31] M. Giomo, A. Buso, P. Fier, G. Sandonà, B. Boye, G. Farnia, Electrochim. Acta 54 (2008) 808–815.
[32] E. Brillas, J. Casado, Chemosphere 47 (2002) 241–248.
[33] B. Chaplin, Environ. Sci.: Processes Impacts 16 (2014) 1182–1203.
[34] E. Brillas, J. Braz. Chem. Soc. 25 (2014) 393–417.
[35] C. Flox, P.L. Cabot, F. Centellas, J.A. Garrido, R.M. Rodríguez, C. Arias, E. Brillas, Appl. Catal. B: Environ. 75 (2007) 17–28.
[36] A. Thiam, I. Sirés, E. Brillas, Water Res. 81 (2015) 178–187.
[37] J.R. Steter, E. Brillas, I. Sirés, Appl. Catal. B: Environ. 224 (2018) 410–418.
[38] A.R.F. Pipi, I. Sirés, A.R. De Andrade, E. Brillas, Chemosphere 109 (2014) 49–55.
[39] F. Gozzi, I. Sirés, A. Thiam, S.C. de Oliveira, A. Machulek Jr., E. Brillas, Chem. Eng. J. 310 (2017) 503–513.
[40] F.C. Moreira, J. Soler, A. Fonseca, I. Saraiva, R.A.R. Boaventura, E. Brillas, V.J.P. Vilar, Appl. Catal. B: Environ. 182 (2016) 161–171.
[41] G. Coria, T. Pérez, I. Sirés, E. Brillas, J.L. Nava, Chemosphere 198 (2018) 174–181.
[42] C. Espinoza, J. Romero, L. Villegas, L. Cornejo-Ponce, R. Salazar, J. Hazard. Mater. 319 (2016) 24–33.
[43] L.C. Almeida, S. Garcia-Segura, N. Bocchi, E. Brillas, Appl. Catal. B: Environ. 103 (2011) 21–30.
[44] E. Isarain-Chávez, R.M. Rodríguez, P.L. Cabot, F. Centellas, C. Arias, J.A. Garrido, E. Brillas, Water Res. 45 (2011) 4119–4130.
[45] S. Garcia-Segura, E. Brillas, Electrochim. Acta 140 (2014) 384–395.
[46] V.S. Antonin, S. Garcia-Segura, M.C. Santos, E. Brillas, J. Electroanal. Chem. 747 (2015) 1–11.
[47] S. Garcia-Segura, E. Brillas, Appl. Catal. B: Environ. 181 (2016) 681–691.
[48] T. Pérez, I. Sirés, E. Brillas, J.L. Nava, Electrochim. Acta 228 (2017) 45–56.
[49] S. Malato, J. Blanco, A. Campos, J. Cáceres, C. Guillard, J.M. Herrmann, A.R. Fernández-Alba, Appl. Catal. B: Environ. 42 (2003) 349–357.
[50] M. Panizza, G. Cerisola, Chem. Rev. 109 (2009) 6541–6569.
[51] A. Zapata, T. Velegraki, J.A. Sánchez-Pérez, D. Mantzavinos, M.I. Maldonado, S. Malato, Appl. Catal. B: Environ. 88 (2009) 448–454.